Universität Potsdam

Fred Feudel, Norbert Seehafer

Bifurcations and pattern formation in a 2D Navier-Stokes fluid

NLD Preprints ; 23

Bifurcations and pattern formation in a 2D Navier–Stokes fluid

F. Feudel and N. Seehafer
Max-Planck-Gruppe Nichtlineare Dynamik, Universität Potsdam, PF 601553, D-14415 Potsdam, Germany

We report on bifurcation studies for the incompressible Navier–Stokes equations in two space dimensions with periodic boundary conditions and an external forcing of the Kolmogorov type. Fourier representations of velocity and pressure have been used to approximate the original partial differential equations by a finite-dimensional system of ordinary differential equations, which then has been studied by means of bifurcation-analysis techniques. A special route into chaos observed for increasing Reynolds number or strength of the imposed forcing is described. It includes several steady states, traveling waves, modulated traveling waves, periodic and torus solutions as well as a period-doubling cascade for a torus solution. Lyapunov exponents and Kaplan–Yorke dimensions have been calculated to characterize the chaotic branch. While studying the dynamics of the system in Fourier space, we also have transformed solutions to real space and examined the relation between the different bifurcations in Fourier space and topological changes of the streamline portrait. In particular, the time dependent solutions, as e.g. traveling waves, torus and chaotic solutions, have been characterized by the associated fluid-particle motion (Lagrangian dynamics).

05.45.+b, 47.20.Ky, 47.27.Cn, 47.54.+r

I. INTRODUCTION

One of the better studied two-dimensional viscous flows is the so-called Kolmogorov flow, where the velocity is everywhere parallel or anti-parallel to a given direction, perpendicular to which it varies sinusoidally. If driven hard enough, of course, this flow becomes unstable [1] (for a recent reconsideration of the stability problem see Ref. [2], where also experimental aspects of the Kolmogorov flow are discussed), and for still harder driving finally a chaotic state is reached, which has been studied by means of numerical simulations [3,4].

Systematic investigations of the qualitative behaviour of solutions to truncations (in Fourier space) of the 2D incompressible Navier–Stokes equations (NSE) with an external forcing of the Kolmogorov type are due to Franceschini and his co-workers [5–8] and Lee [9]. These authors studied in detail the rather complex bifurcation sequence leading from laminar, steady states to chaotic solutions. We have continued the studies of Franceschini and Lee and could find some new aspects (part of them described in a companion paper [10]) concerning both the bifurcation sequence and the physical character of some of the attractors. The aim of this paper is to present the complete bifurcation sequence leading to chaos and to characterize the different solution branches by the associated streamline portraits and fluid-particle motions.

II. BASIC EQUATIONS, TRUNCATION AND FORCING

We start from the equations for an incompressible fluid with constant material properties,

$$\rho\left[\frac{\partial \boldsymbol{v}}{\partial t}+(\boldsymbol{v}\cdot\nabla)\boldsymbol{v}\right]=-\nabla p+\rho\nu\nabla^2\boldsymbol{v}+\boldsymbol{f}, \tag{1}$$

$$\nabla\cdot\boldsymbol{v}=0, \tag{2}$$

where $\boldsymbol{v}$ and p denote fluid velocity and thermal pressure, ρ and ν mass density and kinematic viscosity, and $\boldsymbol{f}$ an external body force. Transforming to non-dimensional quantities according to

$$\begin{aligned}&\boldsymbol{x}\to\boldsymbol{x}/L \text{ (position vector)}, \quad t\to t/\frac{L^2}{\nu},\\ &\boldsymbol{v}\to\boldsymbol{v}/\frac{\nu}{L}, \quad p\to p/\frac{\rho\nu^2}{L^2}, \quad \boldsymbol{f}\to\boldsymbol{f}/\frac{\rho\nu^2}{L^3},\end{aligned} \tag{3}$$

Eq. (1) becomes

$$\frac{\partial \boldsymbol{v}}{\partial t}+(\boldsymbol{v}\cdot\nabla)\boldsymbol{v}=-\nabla p+\nabla^2\boldsymbol{v}+\boldsymbol{f}. \tag{4}$$

The non-dimensional velocity (a typical value of it) corresponds to the conventional Reynolds number, R, provided a characteriztic external length scale (e.g., the scale over which $\boldsymbol{f}$ varies) has been chosen for L. If the non-dimensional external length scale is $l\neq 1$, then $R\approx lV$, with V denoting a typical value of the non-dimensional velocity. R will increase with increasing strength of the forcing. Let F denote a typical value of $|\boldsymbol{f}|$. For weak forcing, when spatial scales much smaller than the external one are not yet excited and energy is dissipated on the scale on which it is injected, $V/l^2\approx F$ and $R\approx l^3F$. For strong forcing, on the other hand, when fluid particles are accelerated practically undamped, so that the forcing term in Eq. (4) is approximately balanced by the inertial term, one expects $R\approx l^{3/2}F^{1/2}$ to be a better estimate.

We restrict ourselves to the 2D case and apply periodic boundary conditions on a square region of side length 2π, which is equivalent to considering the motion on the torus $T^2=[0,2\pi]\times[0,2\pi]$. The mean values of $\boldsymbol{v}$ and consequently also of $\boldsymbol{f}$ are assumed to vanish,

$$\int_{T^2} \boldsymbol{v}\,\mathrm{d}^2\boldsymbol{x} = \boldsymbol{0}, \quad \int_{T^2} \boldsymbol{f}\,\mathrm{d}^2\boldsymbol{x} = \boldsymbol{0}. \tag{5}$$

Let $\boldsymbol{v_k}$, $p_{\boldsymbol{k}}$ and $\boldsymbol{f_k}$ denote the Fourier coefficients of $\boldsymbol{v}$, p and $\boldsymbol{f}$ for wave number $\boldsymbol{k} \in \mathbb{Z}^2$, $\boldsymbol{k} \neq \boldsymbol{0}$. In Fourier space the incompressibility condition, Eq. (2), takes the form

$$\boldsymbol{v_k} \cdot \boldsymbol{k} = 0 \tag{6}$$

and is automatically satisfied if $\boldsymbol{v}$ is expressed in the form

$$\boldsymbol{v_k} = v_{\boldsymbol{k}} \boldsymbol{e_k}, \qquad \boldsymbol{k} \neq \boldsymbol{0}, \tag{7}$$

by means of (real) "polarization" vectors $\boldsymbol{e_k}$ perpendicular to $\boldsymbol{k}$,

$$\boldsymbol{e_k} \cdot \boldsymbol{k} = 0, \quad \boldsymbol{e_k}^2 = 1, \quad \boldsymbol{e_{-k}} = \boldsymbol{e_k}. \tag{8}$$

The last condition in Eq. (8) ensures that

$$v_{-\boldsymbol{k}} = v_{\boldsymbol{k}}^* \tag{9}$$

for real $\boldsymbol{v}(\boldsymbol{x})$ (the asterisk indicates the complex conjugate). By using this representation for $\boldsymbol{v_k}$ we furthermore easily get rid of the pressure term in Eq. (4) and arrive at the following infinite-dimensional system of ordinary differential equations (ODE):

$$\frac{\mathrm{d}v_{\boldsymbol{k}}}{\mathrm{d}t} = -\boldsymbol{k}^2 v_{\boldsymbol{k}} - \mathrm{i} \sum_{\substack{\boldsymbol{p} \in \mathbb{Z}^2 \\ \boldsymbol{p} \neq \boldsymbol{0}, \boldsymbol{k}}} (\boldsymbol{e_p} \cdot \boldsymbol{k})(\boldsymbol{e_{k-p}} \cdot \boldsymbol{e_k}) v_{\boldsymbol{p}} v_{\boldsymbol{k-p}} + f_{\boldsymbol{k}}. \tag{10}$$

$f_{\boldsymbol{k}}$ on the right of Eq. (10) is defined by

$$f_{\boldsymbol{k}} = \boldsymbol{f_k} \cdot \boldsymbol{e_k}. \tag{11}$$

In our numerical calculations we have used an isotropic truncation in wave number space, following Lee [11,9], who segmented the $\boldsymbol{k}$ space into successive rings $n^2 - n < \boldsymbol{k}^2 \leq n^2 + n$, $n = 1, 2, \cdots$. The rings up to $n = 8$ have been taken into account, altogether 112 $\boldsymbol{k}$ vectors, which amounts to studying a system of 224 ODE.

Because of the periodic boundary conditions, the total energy flow through the boundary of the region considered vanishes, so that in order to enable non-trivial time-asymptotic states some kind of external forcing has to be applied. We have used a constant, single-mode forcing at $\boldsymbol{k} = (4, 1)$, with equal strengths in the real and imaginary parts (identical to the single-mode forcing used by Lee [9]):

$$f_{\boldsymbol{k}} = \begin{cases} f \pm \mathrm{i}f & \text{for } \boldsymbol{k} = \pm(4,1) \\ 0 & \text{for } \boldsymbol{k} \neq \pm(4,1) \end{cases} \tag{12}$$

For this special type of forcing the NSE, Eq. (4), is invariant with respect to translations perpendicular to the $\boldsymbol{k}$ vector of the forced mode. Thus in conjunction with the periodic boundary conditions, our problem has a symmetry group isomorphic to the group U(1).

f on the right of Eq. (12) is our bifurcation parameter. Let the inverse of the modulus of the wave number of the forced mode be taken as the external length scale, i.e. $l \approx 1/\sqrt{17}$. The spatial average of $\boldsymbol{f}^2$ is $4f^2$. Thus according to the consideration at the beginning of this Section, $R \approx 3 \cdot 10^{-2} \cdot f$ for weak forcing (appropriate for most of our study) and $R \approx \sqrt{3 \cdot 10^{-2} \cdot f}$ for strong forcing may be taken as estimates for the conventional Reynolds number.

III. STEADY STATES AND TRAVELING WAVES

For very weak forcing a stable stationary solution with only the forced mode excited is the only attracting (i.e., time-asymptotic) state (branch STEADY-1; an overview of the different solution branches is given in Table I). This solution can be analytically expressed in the form

$$\boldsymbol{v}(x, y) = \frac{2f}{17}(\cos(4x + y) - \sin(4x + y))\boldsymbol{e}_{(4,1)}. \tag{13}$$

It represents a shear flow with streamlines parallel to the vector $\boldsymbol{e}_{(4,1)}$, which is perpendicular to the wave lattice vector $\boldsymbol{k} = (4, 1)$ of the forced mode. The direction of the flow changes across the straight lines

$$y = -4x + (n + \frac{1}{4})\pi, \quad n \in \mathbb{Z}. \tag{14}$$

It is evident that the solution given by Eq. (13) retains the translational symmetry in the direction of $\boldsymbol{e}_{(4,1)}$. This simplest steady state loses its stability in a symmetry-breaking bifurcation where two real eigenvalues of the Jacobian matrix become zero. The new stable steady states (branch STEADY-2), in which more than one but not yet all modes are excited, are no longer symmetric and one eigenvalue of the Jacobian matrix is permanently equal to zero along the solution branch. In a further pitchfork bifurcation the remaining modes become different from zero (branch STEADY-3).

In the following we shall characterize the different steady-state branches by their associated streamline portraits. The streamlines of the first steady state, where only the forced mode is excited, are straight lines and the direction of the velocity changes across the neutral lines given by Eq. (14). In Fig. 1 streamlines are drawn for a forcing slightly above the first bifurcation value. Thick lines correspond to zero lines of the velocity stream function. Compared with the first steady-state branch, these lines have been deformed due to the generation of eight vortices. Solid and dashed lines refer to streamlines in regions with clockwise and counter-clockwise rotating vortices, respectively. This topological structure of the streamline portrait exists only over a relatively small interval of the bifurcation parameter and is then transformed into the more stable configuration shown in Fig. 2. This is generated in a process where the zero lines of the velocity stream function are reconnected such as

to delimit two horizontal layers with oppositely rotating vortices. It seems remarkable that both streamline structures belong to the same steady-state branch (STEADY-2). Although in Fourier space no bifurcation is observed, the streamline topology in real space changes qualitatively.

The velocity field corresponding to the third steady-state branch (STEADY-3) is presented in Fig. 3. The number of vortices remains the same, but new closed streamlines have been formed that encircle two and four vortices, respectively.

The third steady-state branch ends up in a special bifurcation where a second eigenvalue in addition to that already vanishing along the whole branch becomes zero. This bifurcation leads to a time-dependent solution where the projection of the modes onto the planes spanned by their respective real and imaginary parts describes circles (with the exception of the forced mode and the modes with wave vectors parallel to that of the forced mode; these modes are still time-independent). This solution may be interpreted as a traveling wave (TW), for which the whole velocity field drifts with a constant speed in the direction of the tanslational invariance of the equations. For a TW the (total) velocity field can be expressed as

$$\boldsymbol{v}(\boldsymbol{x},t) = \sum_{\substack{\boldsymbol{k}\in\mathbb{Z}^2\\ \boldsymbol{k}\neq 0}} A_{\boldsymbol{k}}\boldsymbol{e}_{\boldsymbol{k}} \exp(\mathrm{i}\boldsymbol{k}\cdot(\boldsymbol{c}t+\boldsymbol{x})), \quad A_{\boldsymbol{k}}\in\mathbb{R}, \quad (15)$$

where $\boldsymbol{c}$ represents the velocity of the TW. The streamline structure for the TW at one instant of time is similar to that of the third steady-state branch (cf. Fig. 3), but it is moving constantly parallel to the vector $\boldsymbol{e}_{(4,1)}$. The TW solution loses its stability in a bifurcation which can be explained as a Hopf bifurcation in the co-moving coordinate frame. All the $A_{\boldsymbol{k}}$'s in Eq. (15) become periodic with the same frequency and the resulting solution can be interpreted as a modulated traveling wave (MTW). The forced mode $v_{(4,1)} = A_{(4,1)}$ is no longer constant, but periodic. For any mode not aligned with $\boldsymbol{e}_{(4,1)}$ the projection onto the plane spanned by the real and imaginary parts appears as quasiperiodic with two frequencies, as seen in Fig. 4. The lower frequency corresponds to the circle motion already present for the TW ($\omega = \boldsymbol{k}\cdot\boldsymbol{c}$), while the higher one is related to the modulation (the oscillation of the $A_{\boldsymbol{k}}$'s).

Special properties of the TW and MTW will also be discussed in Sec. IV in the context of the Lagrangian description of the fluid-particle motion.

IV. A SPECIAL ROUTE INTO CHAOS

In the following we shall describe the rest of the bifurcation sequence which finally leads to chaos.

The MTW exists only for a relatively small interval of the bifurcation parameter and bifurcates to a normal torus solution (TORUS-1). In contrast to the MTW, for the new torus branch the forced mode is no longer periodic but quasiperiodic as the other modes. A phase locking at $f = 232.25$ produces a purely periodic solution (PERIOD-1). But this could only be traced up to a value of $f = 273$, where it becomes unstable and trajectories are attracted by another, coexisting branch. We have seen the coexisting branch first for $f = 267.75$ as a second periodic solution. The two periodic solutions look very similar and we suppose a connection of both branches over turning points with an unstable solution in between.

At $f = 270$ the second periodic orbit in turn bifurcates to a torus solution (TORUS-2), for which a phase locking at $f = 282.5$ again leads to a purely periodic solution. At $f = 292.5$ a second frequency (in addition to that of the phase locking) appears, leading to a new torus branch (TORUS-3). This torus solution is degenerate in that, similar to the MTW discussed in Sec. III, the forced mode remains strictly periodic with just one frequency, all other modes being quasiperiodic with two frequencies. We were unable, however, to interpret this solution as an MTW. In Fig. 5 the projection of the torus onto the forced mode is shown. Such a degeneracy may result from a Hopf bifurcation in an invariant subspace without an effect on the forced mode.

Subsequently we have found a period-doubling cascade for this torus solution, namely doublings of the period shown by the forced mode. We could resolve the doublings up to the fourth one; the corresponding trajectory projected onto the forced mode is drawn in Fig. 6.

Although we were unable to prove it exactly, we suppose that the period-doubling cascade is an infinite one leading to chaos. The occurrence of chaos has been verified by calculating the Lyapunov exponents (see Sec. V).

For investigating the fluid motion for the time-dependent solutions a Lagrangian description was necessary, since the streamlines alone give only minor information. If one makes snapshots of the streamlines at different time points, no qualitative changes of the velocity field can be recognized. Even for time-dependent solutions from different branches the streamline structure is nearly the same, qualitatively similar to the velocity field of the third steady state (cf. Fig. 3). We have traced a test particle injected into the fluid by solving its equation of motion,

$$\frac{d\boldsymbol{x}}{dt} = \boldsymbol{v}(\boldsymbol{x},t), \quad \boldsymbol{x}\in\mathbb{R}^2, \quad (16)$$

where $\boldsymbol{v}(x,t)$ is the corresponding solution of the NSE. The periodic boundary conditions for the velocity field have been used to extend the phase space for the fluid particles from our square region into the whole plane $\mathbb{R}^2$.

In Fig. 7 test particle trajectories are shown for several of the time-dependent solutions. For the TW, described in Sec. III, the trajectory results from a superposition of the particle motion along a streamline with the uniform drift (with constant speed $\boldsymbol{c}$, cf. Eq. (15)) of this

streamline. In Fig. 7a the particle has been located on a closed streamline and consequently the trajectory looks like a cylindrical surface. For the MTW a second frequency appears and compared to the TW the trajectory is subject to additional small oscillations (Fig. 7b).

After the generation of the torus branch TORUS-1 the motion has changed completely (cf. Fig. 7c). For a long time the fluid particle is trapped in a ring-like, well separated region, but may suddenly cross the boundary to a neighboring vortex region. In steady states the basins of different vortices are completely separated by heteroclinic lines connecting hyperbolic fixed points. For time-dependent velocity fields, on the other hand, if the motion of fluid particles is studied by means of stroboscopic maps of marked particles (called Poincaré maps), the stable and unstable manifolds of fixed points of these maps may intersect. The penetration of fluid particles through that kind of boundary layers is well described in the theory of mixing [12] and may already occur for two-dimensional time-periodic flows [13]. Fig. 7d gives an example for the motion of a fluid particle in a time-periodic flow belonging to the PERIOD-1 branch. The trajectory looks similar to those shown in Fig. 7c, but the hopping rate is increased. For the TORUS-3 branch (see Fig. 7e), on the other hand, the trajectory is trapped in a bounded region of phase spase. Finally in Fig. 7f a trajectory for the chaotic branch is drawn, where again mixing occurs.

We also have carried out numerical simulations in which two blobs were injected into the chaotic fluid. The blobs are streched and folded, but the mixing process depends strongly on the initial locations of the blobs. In some cases the blobs remain separated, especially if one of them is attracted by one of the smaller eddies surrounding the elliptical zero-velocity points. In other cases a complete mixing was observed. But also in these cases the mixing process needs some time, probably because the velocity field varies on a time scale much larger than that of the fluid-particles motion. A more detailed investigation of this phenomenon is under way.

V. LYAPUNOV EXPONENTS AND KAPLAN–YORKE DIMENSIONS FOR THE CHAOTIC REGIME

For the chaotic branch we have calculated Lyapunov exponents and Kaplan–Yorke dimensions. By using an algorithm of Shimada and Nagashima [14], the largest Lyapunov exponents have been calculated within the interval $325 \leq f \leq 425$, with a stepsize of $\Delta f = 2.5$. In Fig. 8 only those larger than zero are shown (three in the interval considered). It should be mentioned that for all values of the bifurcation parameter two of the Lyapunov exponents are equal to zero. One of them belongs to the direction of the trajectory, the other is related to the continuous symmetry of the system.

The Lyapunov exponents have been used to calculate the Kaplan–Yorke dimension D_{KY} of the attractor, which is a good approximation of its Hausdorff dimension [15]. If the Lyapunov exponents λ_i are ordered descendingly and j is the largest index satisfying

$$\sum_{i=1}^{j} \lambda_i \geq 0, \tag{17}$$

then

$$D_{\mathrm{KY}} = j - \frac{1}{\lambda_{j+1}} \sum_{i=1}^{j} \lambda_i. \tag{18}$$

For the TORUS-3 branch, including the interval of the period-doubling cascade, the dimension is equal to three; the additional dimension (over that of a two-dimensional torus) results from the Lee symmetry of the system. For the chaotic branch there is roughly a linear dependence of the dimension on the bifurcation parameter f (see Fig. 9).

It would be interesting to compare the function in Fig. 9 with analogous calculations for a truncation including much more modes. If the Kaplan–Yorke dimension would be of the same order, these higher modes could be interpreted as slaved modes and the qualitative behaviour of the system would be essentially determined by the lower modes. We shall try to attack this problem in a future study.

VI. CONCLUSION

We have studied bifurcations and patterns in an incompressible 2D Navier–Stokes fluid with periodic boundary conditions and an external forcing in a single Fourier mode. The strength of the forcing has been our bifurcation parameter. Remarkably, qualitative changes of the streamline topology of the fluid in real (2D) space are not necessarily coupled to bifurcations in phase (Fourier) space. For increasing strength of the forcing, the system shows various bifurcations to steady states, traveling waves, modulated traveling waves, periodic and torus solutions, with a final transition to chaos. Deviating from the standard Ruelle–Takens–Newhouse scenario, the transition to chaos occurs via a period-doubling cascade on a degenerate torus branch. This may be a consequence of our special forcing. For the chaotic branch, Lyapunov exponents and Kaplan–Yorke dimensions have been calculated. In the parameter interval we studied, the Kaplan–Yorke dimension depends roughly linearly on the strength of the forcing.

ACKNOWLEDGMENTS

We wish to acknowledge the support by Rüdiger Wolff, Cray Research GmbH Deutschland, in the vectorization of our spectral code.

[1] L. D. Meshalkin and Y. G. Sinai, J. Appl. Math. Mech. **25**, 1700 (1961).
[2] A. Thess, Phys. Fluids A **4**, 1385 (1992).
[3] R. Grappin and J. Léorat, J. Fluid Mech. **222**, 61 (1991).
[4] D. Armbruster, R. Heiland, E. J. Kostelich, and B. Nicolaenko, Physica D **58**, 392 (1992).
[5] C. Boldrighini and V. Franceschini, Commun. Math. Phys. **64**, 159 (1979).
[6] V. Franceschini and C. Tebaldi, J. Stat. Phys. **21**, 707 (1979).
[7] V. Franceschini, C. Giberti, and M. Nicolini, J. Stat. Phys. **50**, 879 (1988).
[8] V. Franceschini and C. Giberti, Theor. Comput. Fluid Dyn. **2**, 185 (1991).
[9] J. Lee, Chaos **2**, 537 (1992).
[10] F. Feudel and N. Seehafer, Chaos, Solitons & Fractals (to appear 1995).
[11] J. Lee, Physica D **37**, 417 (1989).
[12] J. M. Ottino, *The Theory of Mixing: Stretching, Chaos and Transport* (Cambridge Univ. Press, Cambridge, 1989).
[13] H. Aref, J. Fluid. Mech. **143**, 1 (1984).
[14] I. Shimada and T. Nagashima, Progr. Theor. Phys. **61**, 1605 (1979).
[15] J. L. Kaplan and J. A. Yorke, in *Functional Differential Equations and Approximations of Fixed Points*, edited by H. O. Peitgen and H. O. Walther (Springer-Verlag, Berlin, 1979), pp. 228–237.

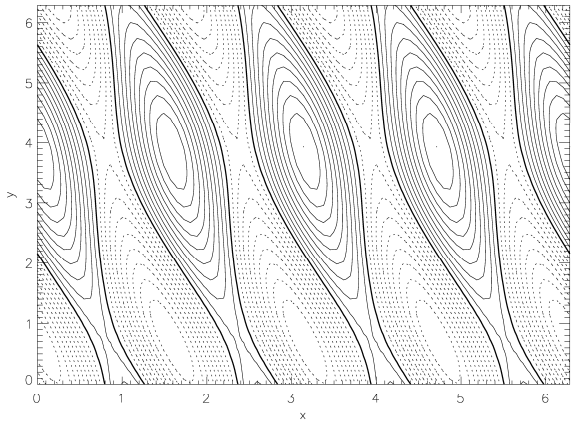

FIG. 1. Streamlines for $f = 52.5$ (branch STEADY-2).

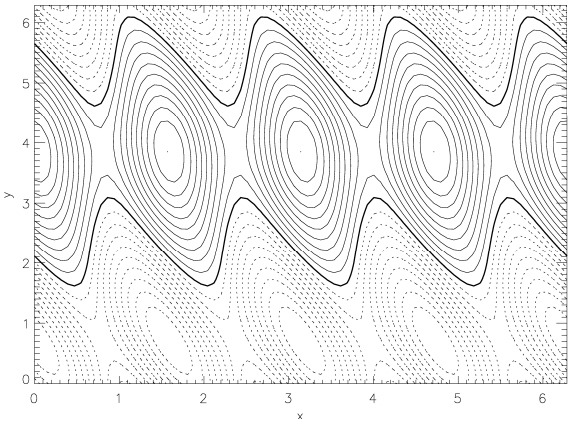

FIG. 2. Streamlines for $f = 55$ (branch STEADY-2).

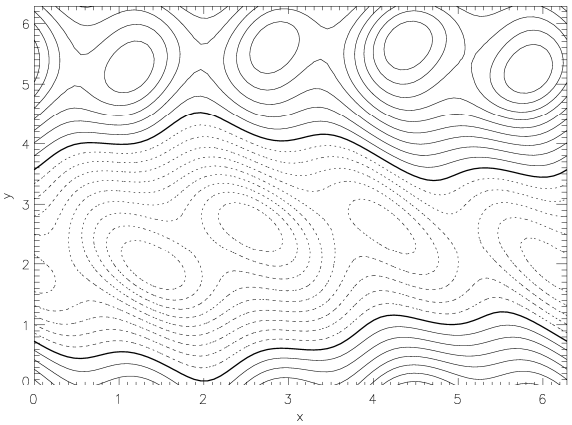

FIG. 3. Streamlines for $f = 170$ (branch STEADY-3).

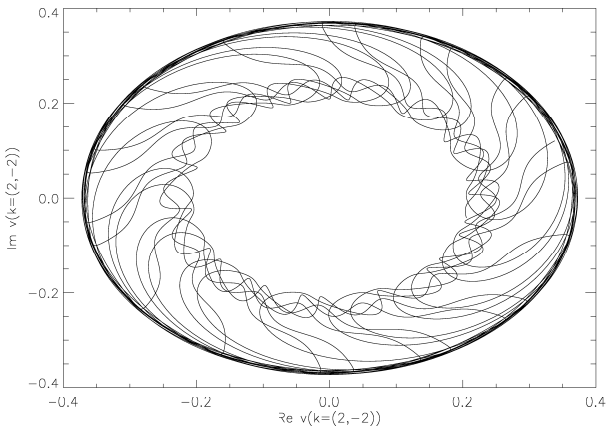

FIG. 4. Projection of the trajectoy for $f = 222.5$ (MTW) onto the real and imaginary parts of the $\boldsymbol{k} = (2, -2)$ mode.

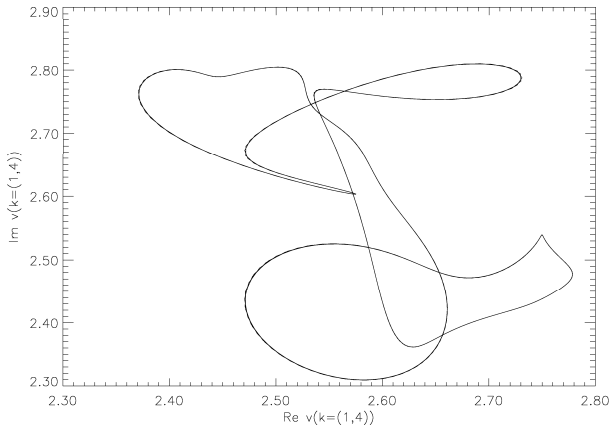

FIG. 5. Projection of the torus TORUS-3 onto the real and imaginary parts of the forced mode $\boldsymbol{k} = (4, 1)$ for $f = 325$.

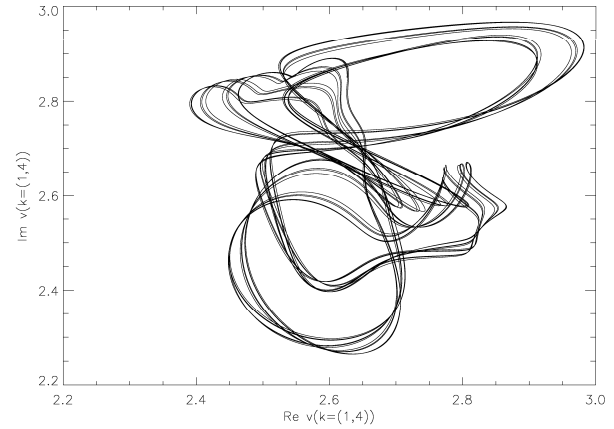

FIG. 6. Projection of trajectory onto the real and imaginary parts of the forced mode $\boldsymbol{k} = (4, 1)$ after the fourth period doubling ($f = 341.75$).

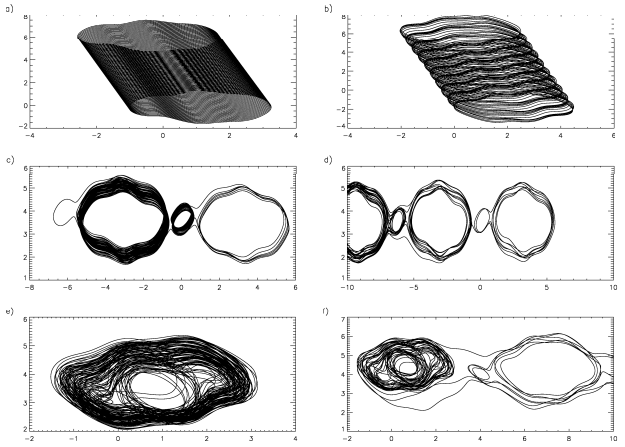

FIG. 7. Trajectory of an injected test particle for a) TW ($f = 207.5$), b) MTW ($f = 222.5$), c) TORUS-1 ($f = 230$), d) Period-1 ($f = 271.25$), e) TORUS-3 ($f = 300$), f) CHAOS ($f = 350$).

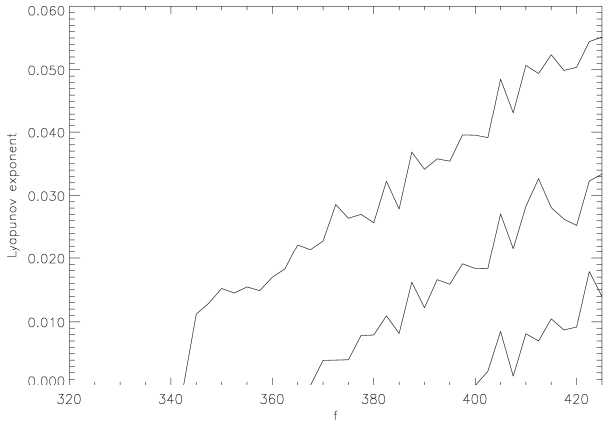

FIG. 8. The Lyapunov exponents larger than zero versus f.

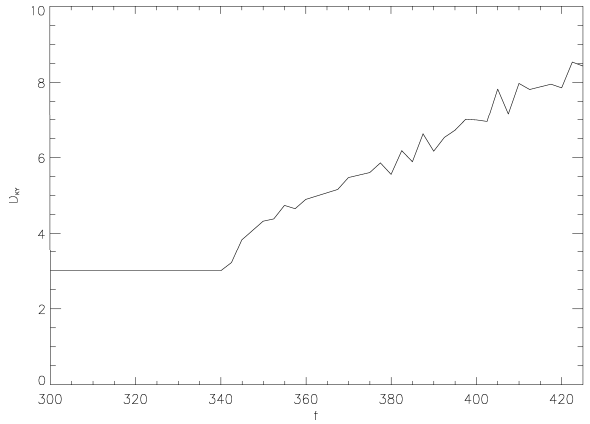

FIG. 9. The Kaplan–Yorke dimension as a function of f.

TABLE I. Overview of the different solution branches

Branch	Interval of stability	Remarks
STEADY-1	$0 < f < 51.5$	Primary symmetric state
STEADY-2	$51.5 < f < 75.25$	Broken symmetry
STEADY-3	$75.25 < f < 176.5$	All modes excited
TW	$176.5 < f < 217.5$	Traveling wave
MTW	$217.5 < f < 230.0$	Modulated traveling wave
TORUS-1	$230.0 < f < 232.25$	Torus
PERIOD-1	$232.25 < f < 273.0$	Phase locking
PERIOD-2	$267.75 < f < 270.0$	Coexisting periodic orbit
TORUS-2	$270.0 < f < 282.5$	Torus
PERIOD-3	$282.5 < f < 292.5$	Phase locking
TORUS-3	$292.5 < f < 345.0$	Torus, period doubling
CHAOS	$f > 345.0$	Chaotic branch